



**HAL**  
open science

## **Number of independent measurements required to obtain reliable mean scattering properties of irregular particles having a small size parameter, using microwave analogy measurements**

Jean-Baptiste Renard, Jean-Michel Geffrin, Vanesa Tobon Valencia, Hervé Tortel, François Ménard, Pascal Rannou, Julien Milli, Gwenaël Berthet

### ► To cite this version:

Jean-Baptiste Renard, Jean-Michel Geffrin, Vanesa Tobon Valencia, Hervé Tortel, François Ménard, et al.. Number of independent measurements required to obtain reliable mean scattering properties of irregular particles having a small size parameter, using microwave analogy measurements. *Journal of Quantitative Spectroscopy and Radiative Transfer*, 2021, 272, pp.107718. <10.1016/j.jqsrt.2021.107718>. <insu-03255038>

**HAL Id: insu-03255038**

**<https://insu.hal.science/insu-03255038v1>**

Submitted on 10 Jun 2021

HAL is a multi-disciplinary open access archive for the deposit and dissemination of scientific research documents, whether they are published or not. The documents may come from teaching and research institutions in France or abroad, or from public or private research centers.

L'archive ouverte pluridisciplinaire HAL, est destinée au dépôt et à la diffusion de documents scientifiques de niveau recherche, publiés ou non, émanant des établissements d'enseignement et de recherche français ou étrangers, des laboratoires publics ou privés.



HAL Authorization

# Number of independent measurements required to obtain reliable mean scattering properties of irregular particles having a small size parameter, using microwave analogy measurements

Jean-Baptiste Renard<sup>1</sup>, Jean-Michel Geffrin<sup>2</sup>, Vanesa Tobon Valencia<sup>2</sup>, Hervé Tortel<sup>2</sup>, François Ménard<sup>3</sup>, Pascal Rannou<sup>4</sup>, Julien Milli<sup>3</sup>, Gwenaël Berthet<sup>1</sup>

1. LPC2E, CNRS - Université d'Orléans - CNES, Orléans, France

2. Aix Marseille Université, CNRS, Centrale Marseille, Institut Fresnel, Marseille, France

3. Université Grenoble Alpes, CNRS, IPAG, Grenoble, France

4. GSMA - Université de Reims, Reims, France

**Abstract.** Laboratory measurements of light scattered by a cloud of randomly oriented levitating particles are often used to interpret remote sensing measurements of dust in space and in Earth's atmosphere. It is necessary to know how many particles or how many different orientations of the same particles must be considered to retrieve the mean scattering function of brightness and polarization. New laboratory measurements were conducted using the microwave analogy method between frequencies of 3 to 18 GHz, where an "analog" particle with a small size parameter in a range of 0.5-12 will have a size of several cm. Twelve such "analog" particles from compact shapes to aggregates with small fractal dimensions were fabricated by additive manufacturing (3D printing) and were studied. The number of necessary measurements to reach the mean scattering properties of a particle with an accuracy of about 5% is obtained for less than 20 different orientations. To reach a 1.5% ( $1-\sigma$ ) error in brightness and a 0.5% ( $1-\sigma$ ) error in polarization, the number of necessary measurements is in a range of 20 to 70, depending on the shape, fluffiness, deviation from a perfect sphere, and surface irregularities of the particle. These results show that several tens of randomly oriented particles of the same size are sufficient to retrieve the mean light scattering properties. Also, several tens of orientations of the same particles provide mean scattering properties, compared to modelling calculations using the Finite Element Method, for an aggregate composed of identical monomers.

## 1. Introduction

Laboratory measurements of light scattered by a cloud of irregular particles are necessary to interpret the brightness and polarization remote sensing measurements of comets, interplanetary dust cloud, and circumstellar material orbiting stars, e.g., protoplanetary and debris disks. Such comparisons are conducted to retrieve bulk physical properties of particles such as composition, size distribution, albedo, and porosity [1-6]. The analyses often assume that the observed particles are randomly oriented inside the cloud, as well as during the reference laboratory measurements. On the opposite, the possible orientation of grains, like in a gas flow or in case of strong magnetic field [7], can modify the scattering properties of an ensemble of particles. Such changes have been shown by [8] during laboratory measurements where the particles were carried and aligned by an airflow, and thus are not considered in this work.

47 Several databases of laboratory measurements provide optical properties (phase or  
48 scattering functions in intensity and in polarization) of levitating particles having the same size  
49 and composition, obtained by different techniques at ground or during microgravity  
50 conditions [9-14]. Such experiments, for particles having small to large size parameters ( $\pi D/\lambda$ ,  
51 where  $D$  is the diameter and  $\lambda$  is the wavelength), assume that indeed they are randomly  
52 oriented and that enough particles are considered during the measurements, from tens to  
53 hundreds or thousands, to retrieve the mean optical properties. As an example, 54 different  
54 orientations of the same millimetre-sized particle have been considered by [5] to retrieve the  
55 mean scattering properties. Nevertheless, the authors have not quantified in detail how many  
56 particles with different orientations are needed to achieve such conditions. Similarly, aerosol  
57 counters used in the atmosphere to count and determine the size distribution of the solid  
58 particles empirically consider their effective optical properties [16-18]. This approach works  
59 well for the submicron particles that are often in large concentrations (more than tens of  
60 particles  $\text{cm}^{-3}$ ) but some uncertainties in size determination can arise when the concentrations  
61 are too low because not enough particles are detected. Finally, experiments and numerical  
62 calculations that consider individual irregularly shaped particle need also to know how many  
63 different orientations are needed to establish the mean optical properties.

64 Although theoretical approaches have been proposed [15], experimental approach can  
65 also be conducted to determine how many particles randomly oriented, or how many  
66 different orientations of the same particle, are indeed necessary to access the mean scattering  
67 properties reliably. This approach is difficult to conduct for particles with a small size  
68 parameter typically in the range of 0.5-12, which corresponds to particles between 0.1 to 2.5  
69  $\mu\text{m}$  size in the visible domain. Such particles levitated by an air draught or during microgravity  
70 conditions could aggregate, preventing to sustain a cloud of individual particles.

71 Instead of using real particles, an alternative consists in using the microwave analogy  
72 [19-24] and individual particles that can be easily manipulated to control their shape and  
73 orientations. The aim will be to measure the properties of a single particle at numerous  
74 orientations to figure out its mean properties to mimic an ensemble of specific particles that  
75 would be randomly oriented. With that concept, particles of the order of 1  $\mu\text{m}$  in the visible  
76 domain are of several cm when studied at a frequency of several GHz, although the size  
77 parameter is conserved. Many electromagnetic scattering measurements can be conducted  
78 with a single particle by changing only its orientation with respect to the incident radiation  
79 beam. Such particles can be built in various materials using a 3-D printer. The permittivity of  
80 a given material, or its (complex) refractive index, which is the square root of the (complex)  
81 permittivity, can be chosen to reproduce the optical properties of real particles that can be  
82 found in space and in Earth's atmosphere.

83  
84

## 85 **2. Conditions of microwave analogy measurements**

86

87 The measurements are conducted in the anechoic chamber at the "Centre Commun  
88 de Ressources en Microondes" (CCRM, Institut Fresnel, Marseille, France). Features and  
89 performances are given in [25]. Briefly, the device operates for this study at 16 frequencies  
90 from 3 to 18 GHz. The use of 16 frequencies from 3 to 18 GHz allows us to explore a range of  
91 size parameters that vary by a factor of six for the same particle, with a refractive index that  
92 can be considered almost constant for the chosen materials. The angle between the emitter  
93 and receiver antennas is changed from one measurement to another, by steps of  $2^\circ$ , to obtain

94 the scattering function in scattering angles from  $-130^\circ$  to  $130^\circ$ . The sample, mounted at the  
 95 centre of the device, can be rotated after one session of measurements, to start a new session  
 96 with another orientation. For the present study, measurements with 36 different orientations  
 97 uniformly distributed from  $-180^\circ$  to  $+170^\circ$  were conducted by a rotation along the vertical axis  
 98 in steps of  $10^\circ$ . The particles are placed on a polystyrene mast; then the rotation axis is vertical,  
 99 *i.e.* parallel to the mast. The particles are placed first according to their greatest length  
 100 (horizontally), then to their smallest length (vertically), and at about  $45^\circ$  (slanted) when more  
 101 measurements are necessary (named inclinations in the following).

102 The device records the amplitude and the phase of the perpendicular and parallel  
 103 scattered electric fields. The polarized scattering intensity  $I_{\text{perp}}$  and  $I_{\text{par}}$  with respect to the  
 104 scattering plane (also so-called *S* and *P*), are the square of the amplitudes, and are used to  
 105 retrieve the scattering (or phase) function for the intensity *I* and for the polarisation *P*  
 106 (formulas 1 and 2).

107

$$108 \quad I = I_{\text{perp}} + I_{\text{par}} \quad (1)$$

$$109 \quad P (\%) = 100 \times (I_{\text{perp}} - I_{\text{par}}) / (I_{\text{perp}} + I_{\text{par}}) \quad (2)$$

110

111 Twelve different samples having a large variety of size, shapes, porosities and fractal  
 112 dimensions have been studied, which can be representative of the main particle families that  
 113 can be found in space and Earth's atmosphere. Since particles with different sizes are  
 114 considered, the present study covers a size parameter range of 0.5 -12. Figure 1 presents the  
 115 shape of the particles for which some physical parameters are given in table 1. The definition  
 116 of the diameter is not easy in case of fluffy particles and particles with low fractal dimension,  
 117 thus we provide both the gyration diameter and the equivalent diameter calculated from  
 118 mean projected surface area. The size parameter is calculated from the gyration diameter for  
 119 the fractal particles (AgC series except AgC181, and SootAcry) and from the equivalent  
 120 diameter for the compact particles (AgC181, gravels and rough spheres).

121 For the AgC232, AgC233, AgC185, AgC186 and AgC187, the diameter of the monomer  
 122 is 5.5 nm. The "SootAcryl" sample is based on a numerically generated analogue of a soot  
 123 aggregate mimicking necking and overlapping phenomenon [26]. The rough spheres are  
 124 derived from a perfect sphere meshed with triangles, and then perturbed modifying the  
 125 distance  $d(\text{OV}_i)$ , with a random perturbation:

126

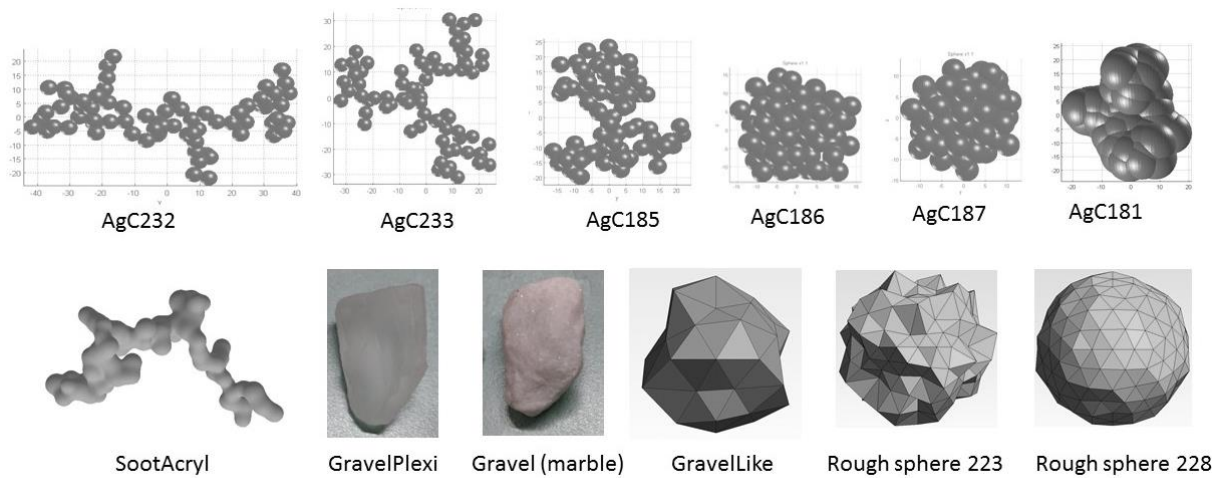
$$127 \quad d(\text{OV}_i) = R + a \cdot \text{rand}(i) \quad (3)$$

128

129 where  $d(\text{OV}_i)$  is the distance from the center of the sphere *O* to the vertex *V<sub>i</sub>* of the triangles,  
 130 *rand* is a random number between -1 and 1, and *R* is the radius of the original sphere (16.25  
 131 mm). For the "Rough Sphere 233"  $a = 3.75$  mm, and for the "Rough Sphere 228"  $a = 0.75$  mm.  
 132 The roughness of the sphere and the deviation from sphericity can be estimated by the ratio  
 133  $D_i/D_v$ , where  $D_v$  corresponds to the diameter of the smaller compact sphere containing the  
 134 same amount of material as the particle and  $D_i$  corresponds of the diameter of the sphere  
 135 containing the particle.

136 All the particles are made by additive manufacturing using an acrylate-based resin,  
 137 except the two gravels that are made of Plexiglas and marble (having similar shapes). The  
 138 mean refractive index of the particles made of acrylate was measured to be  $1.7 + 0.03i$  (which  
 139 can be representative of some carbonaceous particles [27] but also of astrosilicate particles  
 140 [28]), the refractive index of the Plexiglas is of  $1.6 + 0.01i$ , and the refractive index of the

141 marble is assumed to be of  $2.9 + 0.2i$  for all the frequencies (which is representative of strongly  
 142 optically absorbent particles).  
 143



144  
 145 *Figure 1: The studied samples (not on the same scale, see table 1 for the size of the samples)*  
 146

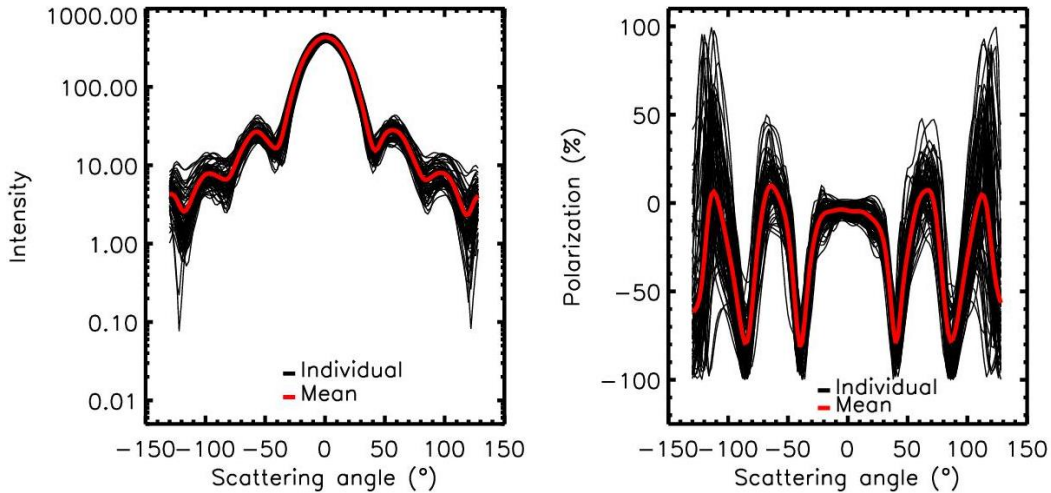
Sample	Box containing the particle (mm <sup>3</sup> )	Gyration diameter (mm)	Equivalent diameter (mm)	Fractal dimension	Dv	Di	Di/Dv
AgC232	76 x 74 x 62	64	39	1.5	23.0	76	3.3
AgC233	61 x 39 x 67	48	37	1.7	22.9	67	2.9
AgC185	41 x 43 x 49	34	34	2.0	23.0	49	2.1
AgC186	34 x 35 x 34	23	31	2.5	23.0	34	1.5
AgC187	29 x 29 x 29	20	27	2.8	23.0	29	1.3
AgC181	46 x 28 x 50	-	40	-	35.9	50	1.4
SootAcryl	66 x 48 x 22	41	32	1.8	22.7	68.3	3.0
GravelPlexi	14 x 20 x 18	-	17	-	14.8	24.6	1.7
Gravel(marble)	14 x 20 x 18	-	17	-	17.0	25.3	1.5
GravelLike	32 x 34 x 38		32		30.6	38	1.2
Rough sphere 223	40 x 40 x 40	-	36	-	31.9	40	1.3
Rough sphere 228	34 x 34 x 34	-	34	-	32.2	34	1.05

147 *Table 1: Physical parameters of the samples. The gyration diameters and the fractal*  
 148 *idimensions are calculated assuming that the spheres are not interpenetrated; the Dv*  
 149 *corresponds to diameter of the smaller compact sphere containing the same amount of*  
 150 *material as the particle; Di corresponds to the diameter of the sphere containing the particle*  
 151

152  
 153 **3. Method of measurement analysis**

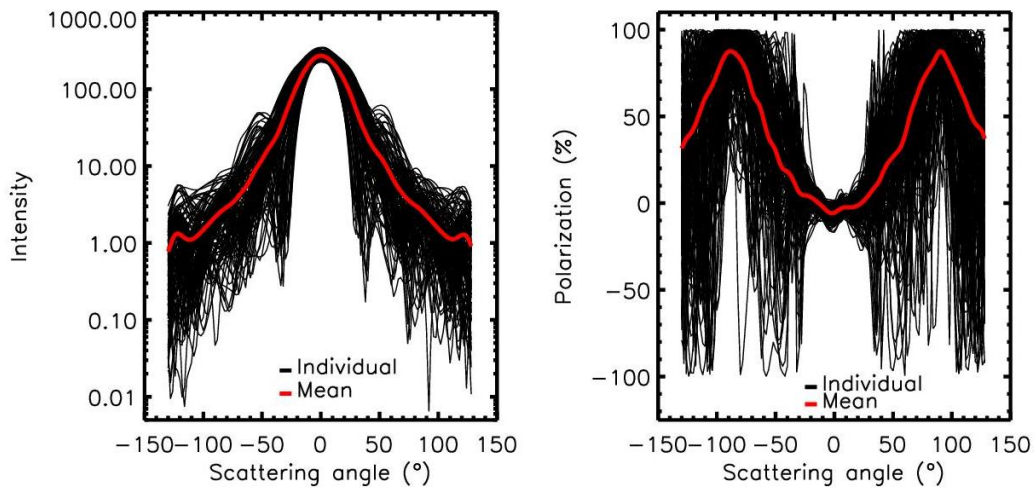
154  
155  
156  
157  
158  
159  
160  
161  
162  
163

Individual measurements of the scattering function (intensity and polarization) can exhibit strong oscillations; these oscillations are stronger as the particles are highly irregular. Figures 2 and 3 show examples of such oscillations for the rough sphere 223 and for the AgC185 at a frequency of 12 GHz, which corresponds to a size parameter of  $\sim 4.5$ . The amplitude of the dispersion for intensity at large scattering angles is of the order of 10 for the rough sphere while the amplitude dispersion can reach a factor of 100 for the AgC185. For the polarization, the dispersion can reach at some angles the minimal and maximal possible values (-100 and 100%).



164  
165  
166  
167  
168  
169

*Figure 2: Individual scattering functions for the rough sphere 223 (left: intensity; right: polarization) for the individual measurements at a given orientation and the mean of all the scattering functions*



170  
171  
172  
173  
174  
175

*Figure 3: Individual scattering functions for the AgC185 (left: intensity; right: polarization) for the individual measurements at a given orientation and the mean of all the scattering functions*

176 To determine how many measurements are necessary to retrieve a mean scattering  
177 function for intensity and polarization with a given accuracy, tens of individual measurements  
178 with different orientations must be considered. The procedure is different for intensity and  
179 polarization because intensity is directly retrieved from the sum of polarized measurements  
180 while polarization is a relative parameter always retrieved from the ratio between the  
181 difference and the sum of polarized intensity measurements and is given in a range from -  
182 100% to 100%.

183 For the intensity, we calculated the mean scattering functions using a given number of  
184 measurements with different orientations. At each scattering angle  $\theta$  we calculate the  
185 difference  $Db(N, \theta)$  between the mean value of the intensity obtained for N measurements  
186 and the mean value obtained for N-1 measurements, divided by the mean value of the  
187 intensity for N measurements; this division act as a normalization to be able to consider  
188 simultaneously the results coming for all scattering angles. Then for each value of N, we  
189 calculate the standard deviation (hereafter called SDB(N)) of the normalized intensity  
190 differences obtained for all scattering angles. This standard deviation, which can represent  
191 the  $1-\sigma$  uncertainty of the resulting mean intensity values, must decrease while the number  
192 of measurements increases. This procedure can be expressed as follows:

$$193 \quad Db(N, \theta) = ( \sum_1^N B(\theta) - \sum_1^{N-1} B(\theta) ) / \sum_1^N B(\theta) \quad (4)$$

$$194 \quad SDB(N) = \sigma(Db(N, \theta)) \quad (5)$$

195

196 with N the number of measurements, B the intensity and  $\theta$  the scattering angle.

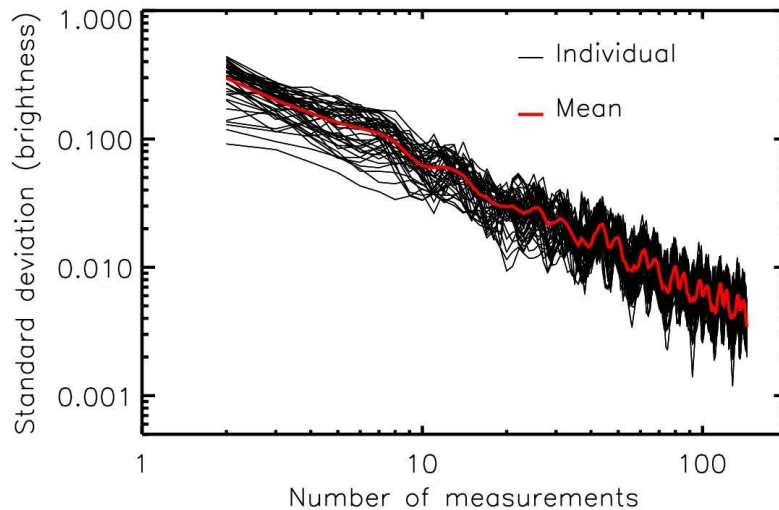
197 To ensure a random distribution of the orientation when calculating the  $Db(N, \theta)$   
198 parameter, the calculation is conducted for different combinations on the angular orientation  
199 and the inclination of the sample; then the results for SDB(N) are averaged. The choice of the  
200 first orientation and the selection of the following orientations (randomly distributed or  
201 considering increasing angles) do not statistically change the results for the number of  
202 necessary measurements that remains within a  $\pm 15\%$  uncertainty.

203 As a first step to visualise the sensitivity to the number of measurements, Figure 4  
204 presents the evolution of the standard deviation with the number of measurements (the plot  
205 is based on the rotation of the particles around different axes). The frequencies here  
206 considered are above the Rayleigh scattering regime (size parameter greater than about 2.5  
207 [29]) and different combinations of orientations and inclinations of the AgC185 sample. In log-  
208 log scale, the trend is almost linear, indicating that it could be fitted by a power law that will  
209 depend on the studied sample (exponent typically in the -0.8- 1.1 range).

210 Three different domains can be defined; firstly, the standard deviation decreases  
211 strongly to reach an accuracy of 0.05 (*i.e.* 5%) for about 15 different orientations, secondly the  
212 standard deviation slowly decreases for a number of measurements up to about 70 producing  
213 a mean intensity uncertainty of about 0.01 (*i.e.* 1%), and thirdly the standard deviation slightly  
214 decreases producing a mean intensity uncertainty below 0.01 (*i.e.* 1%). Increasing the number  
215 of measurements will reduce again the uncertainties, but such approach does not seem  
216 necessary since we can admit that a  $1-\sigma$  accuracy of the order of 1% is sufficient for the  
217 interpretation of the intensity measurements.

218

219



220  
 221 *Figure 4: Evolution of the standard deviation with the number of measurements for the*  
 222 *intensity of the AgC185 sample; the black lines represent the results for the different*  
 223 *frequencies and the different combinations of orientations and inclinations; the red line*  
 224 *represents the mean value*

225  
 226  
 227 For the polarization, the sums of the N orthogonal and parallel polarized scattering  
 228 components are first calculated, then the polarization is calculated. The  $D_p(N, \theta)$  parameter  
 229 is calculated by the difference between the polarization obtained for N measurements and  
 230 the polarization obtained for N-1 measurements. Finally, the SDP(N) parameter corresponds  
 231 to the standard deviation of  $D_p(N, \theta)$  for all scattering angles, which corresponds to the  
 232 polarization uncertainty at 1- $\sigma$  in absolute value (%). This procedure can be expressed as  
 233 follows:

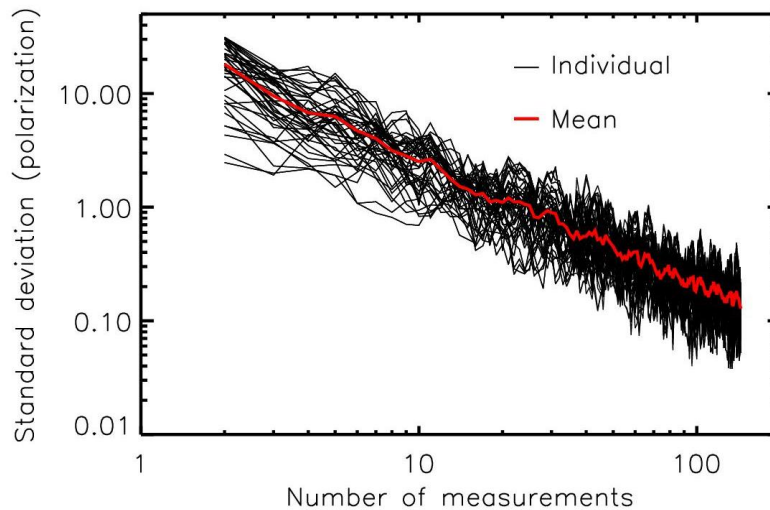
234  
 235 
$$P(N, \theta) = 100 \cdot (\sum_1^N I_{\text{perp}}(\theta) - \sum_1^N I_{\text{par}}(\theta)) / (\sum_1^N I_{\text{per}}(\theta) + \sum_1^N I_{\text{par}}(\theta)) \quad (6)$$

236 
$$D_p(N, \theta) = P(N, \theta) - P(N - 1, \theta) \quad (7)$$

237 
$$\text{SDP}(N) = \sigma(D_p(N, \theta)) \quad (8)$$

238  
 239 Similar trends as those for the intensity are obtained for the polarization  
 240 measurements, as shown in Figure 5 for the AgC185 sample. A 5% uncertainty is obtained for  
 241 about 10 orientations, while about 50 different orientations are necessary to achieve an  
 242 uncertainty of about 0.5% (1- $\sigma$ ); such last value is of the order of the error bars obtained for  
 243 some laboratory measurements with real particles [1,13]

244



245 *Figure 5: Evolution of the standard deviation for the polarization with the number of*  
 246 *measurements of the AgC185 sample; the black lines represent the results for the different*  
 247 *frequencies and the different combinations of orientations and inclinations; the red line*  
 248 *represents the mean value*  
 249

## 252 4. Mean scattering functions and evolution with the size parameter

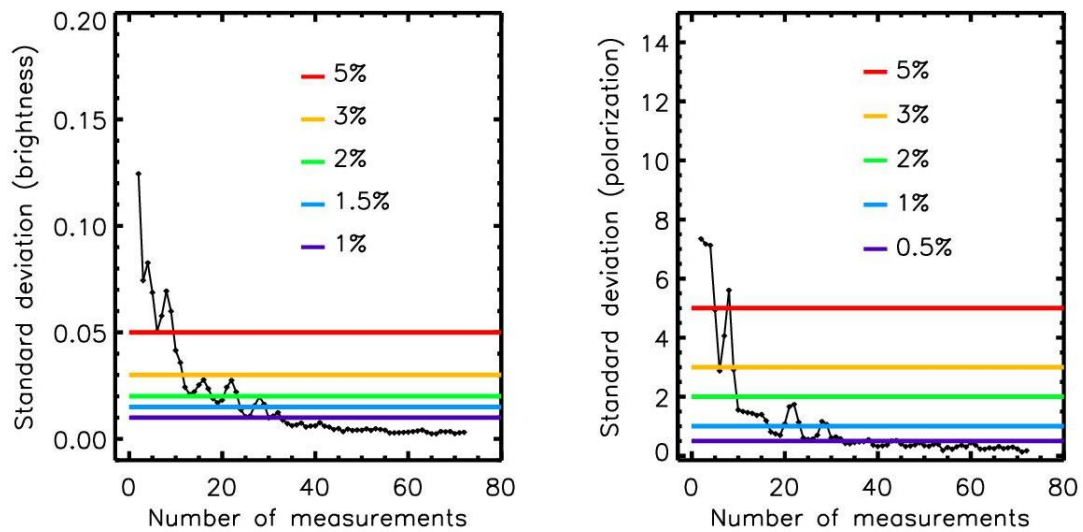
### 254 4.1 Measurements

255  
 256 For a perfect sphere, the scattering properties can be easily retrieved using Mie  
 257 scattering calculations and there is no need for several different orientations of the particle  
 258 When the roughness and/or the deviation from sphericity of the particle increases, increasing  
 259 the number of measurements with different orientations of the particle is needed to retrieve  
 260 the mean properties.

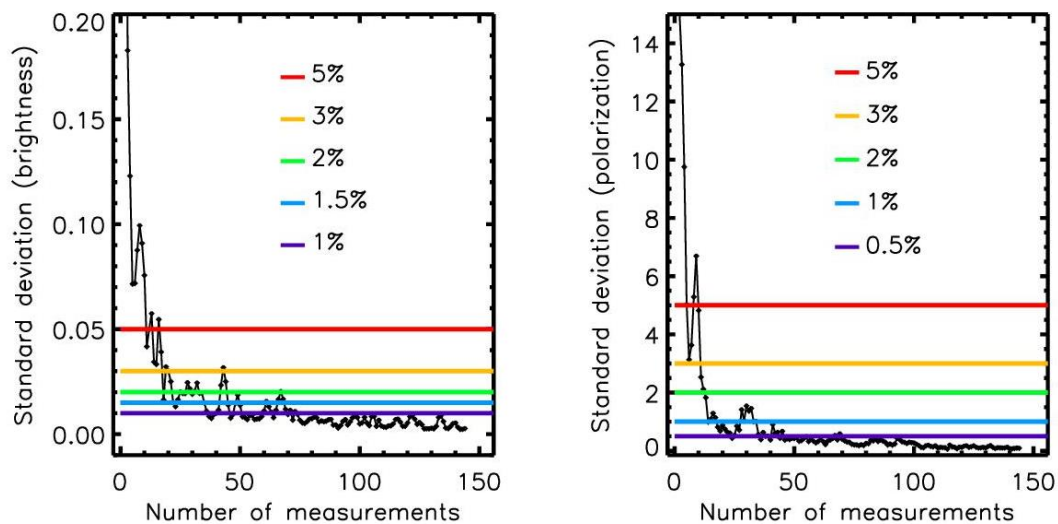
261 Previous results were calculated for all frequencies above the Rayleigh regime. It is of  
 262 interest to conduct the studies at each frequency to retrieve the evolution of the standard  
 263 deviation with the particles' size parameter. For each sample and for all frequencies, the  
 264 number of necessary measurements where the standard deviation of the intensity drops  
 265 below 5%, 3%, 2% 1.5% and 1% is searched for. Similarly, the number of necessary  
 266 measurements where the standard deviation of the polarization drops below 5%, 3%, 2%, 1%  
 267 and 0.5% is searched for. The lower values of 1% for intensity and 0.5 % for polarization are  
 268 arbitrarily chosen but they can correspond to the typical accuracies often achieved when  
 269 performing laboratory measurements with levitating particles in the visible spectral domain.  
 270 All the results for the number of necessary measurements obtained for the different sample  
 271 inclinations (horizontally, vertically, slanted) remains in the  $\pm 15\%$  range for all the standard  
 272 deviation thresholds presented above.

273 Figures 6 and 7 present examples of the evolution of the standard deviations with  
 274 number of measurements for the rough sphere 223 and the AgC185, having a size parameter  
 275 of 4.5. In these examples, the 1% threshold for intensity is reached for about  $35 \pm 5$  and  $100 \pm 15$   
 276 measurements for the rough sphere 223 and the AgC185, respectively. These values decrease  
 277 to  $30 \pm 5$  and  $70 \pm 10$  for the 1.5% threshold. The 0.5% threshold for the polarization is reached  
 278 for  $40 \pm 5$  and  $70 \pm 10$  for the rough sphere 223 and the AgC185, respectively. These first results  
 279 indicate that the number of necessary measurements to retrieve the mean optical properties

280 (hereafter called necessary measurements) is higher in the case of a non-compact particle  
 281 compared to a compact one.  
 282

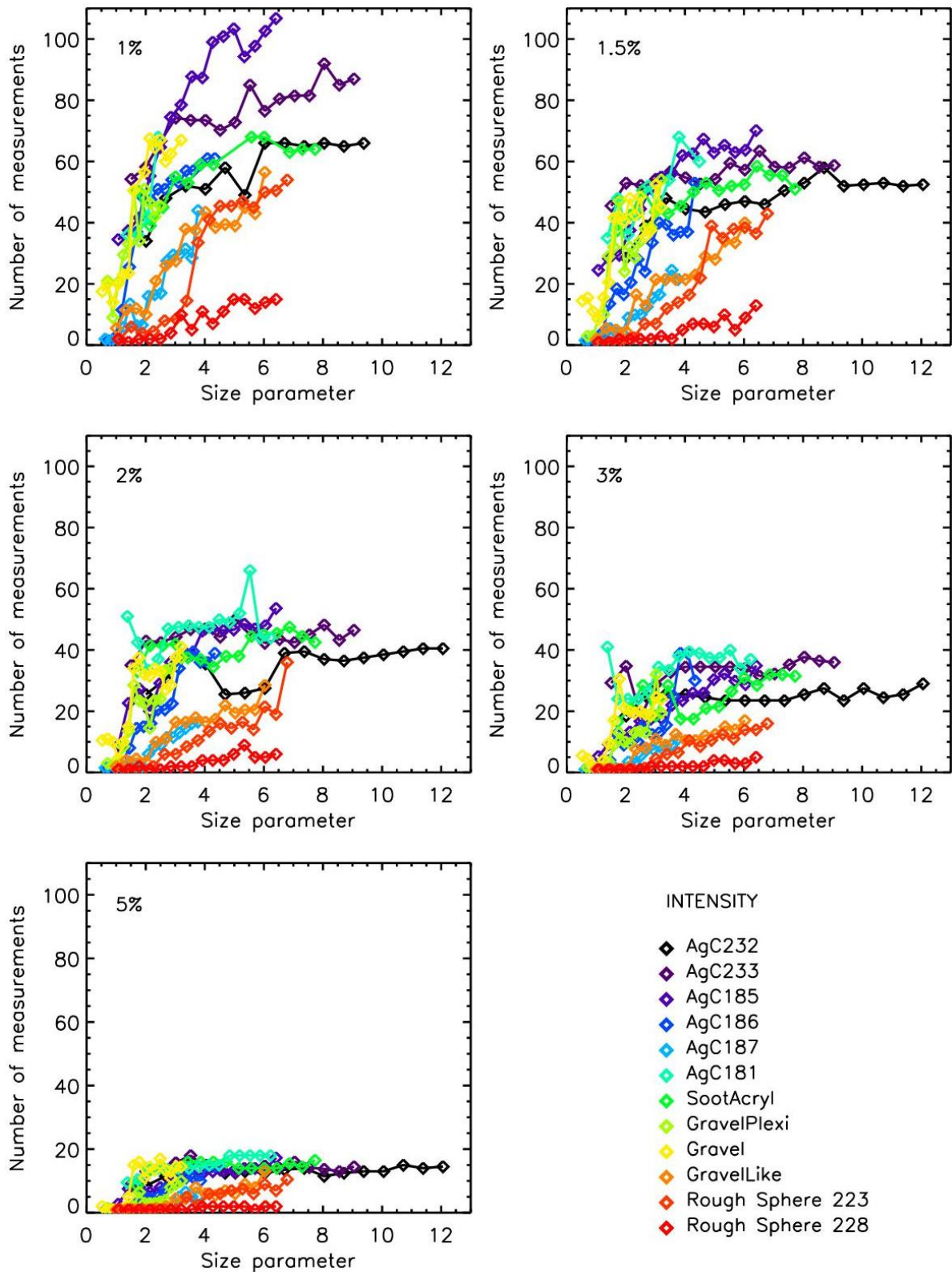


283  
 284 *Figure 6: Example of the evolution of the standard deviation for the intensity and polarization*  
 285 *with the number of measurements for the rough sphere 223, at a size parameter of 4.5.*  
 286



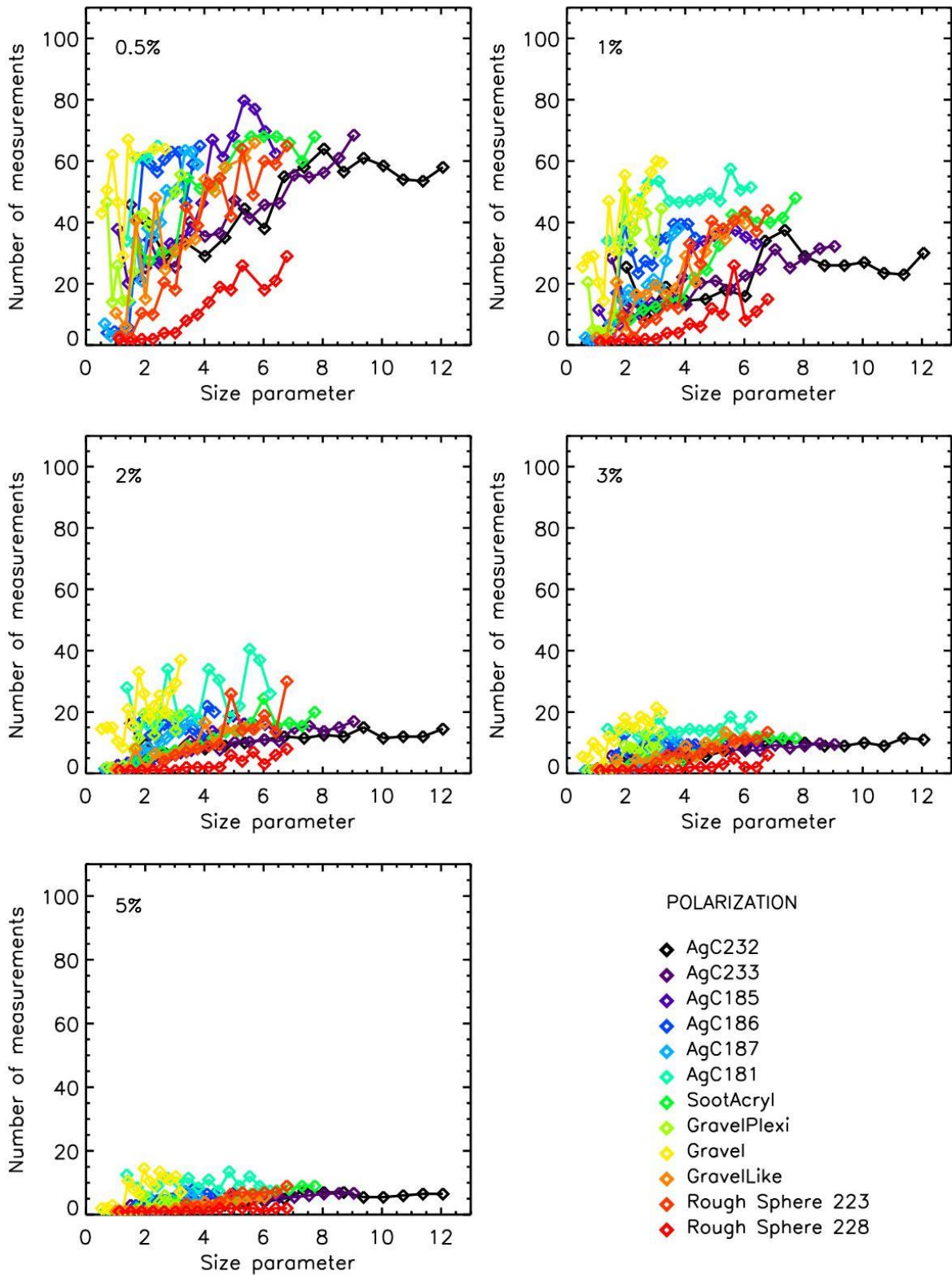
287  
 288 *Figure 7: Example of evolution of the standard deviation for the intensity and polarization*  
 289 *with the number of measurements for the AgC185, at a size parameter of 4.5.*  
 290

291  
 292 The evolution of the number of necessary measurements with size parameter for all  
 293 the samples is presented in Figure 8 for the intensity and in Figure 9 for the polarization,  
 294 considering the different levels of expected accuracy. Obviously, the number of necessary  
 295 measurements is lower when the uncertainties is higher, and less than 20 orientations are  
 296 necessary to retrieve the mean intensity and polarization phase curve with an accuracy of 5%.  
 297 It also decreases with decreasing size parameter; the decrease is steeper for a size parameter  
 298 below 3, corresponding to size particles below the wavelength, and is almost stable for a size  
 299 parameter greater than 5. The number converges towards only one necessary measurement  
 300 when the measurements are performed in the Rayleigh scattering domain.  
 301



302  
 303  
 304  
 305  
 306  
 307  
 308

Figure 8: Evolution of the number of necessary measurements with size parameters, to retrieve the mean intensity scattering properties, for different thresholds of uncertainties (the error bars of  $\pm 15\%$  for the number of necessary measurements are omitted for clarity).



309  
 310  
 311  
 312  
 313  
 314

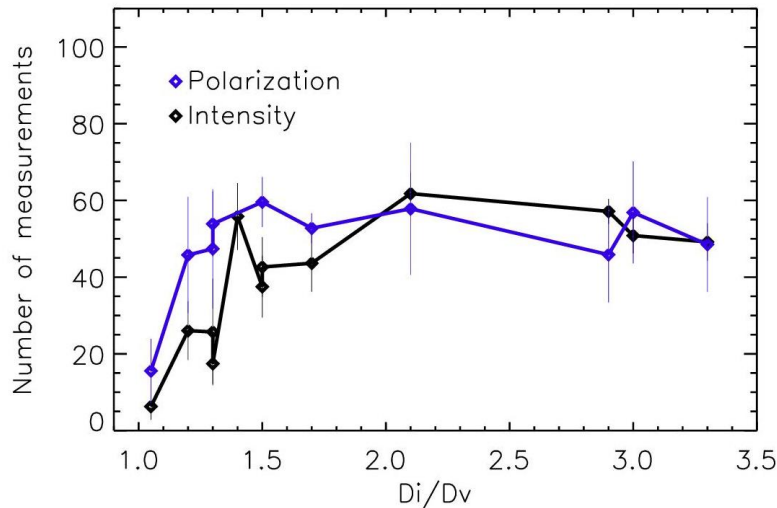
*Figure 9: Evolution of the number of necessary measurements with size parameters, to retrieve the mean polarization scattering properties, for different thresholds of uncertainties (the error bars of  $\pm 15\%$  for the number of necessary measurements are omitted for clarity).*

315 The evolution of the necessary number of measurements to reach a given accuracy  
316 strongly depends on the nature of the particles. As expected, the lower numbers (around 20  
317 for intensity measurements) are obtained for the near-perfect compact sphere rough sphere  
318 228, having rugosity in the  $[\lambda/6, \lambda/33]$  range. Then, the value increases as the surface of the  
319 particles become more irregular (rough sphere 223, GravelLike and AgC187) and the shape  
320 departs from a sphere. The rough sphere 223 has a particular behaviour, starting from values  
321 close to those of the rough sphere 228 for the smallest size parameters and reaching values  
322 of more irregular particles for the largest size parameters. This can be understood when  
323 considering that roughness depends on the frequencies in the  $[\lambda, \lambda/7]$  range. The other  
324 compact particles (Gravel, GravelPlexi, AgC181) and fractal particles (AgC186, SootAcryl,  
325 Agc185, Agc232, AgC233) exhibits similar behaviour with the number of necessary  
326 measurements in the 40-60 range (mean of 50) for intensity measurements. This  
327 categorization for the particles is less obvious when considering the polarization, where only  
328 the rough sphere 228 presents a behaviour that stands out from the other sample.

329 For non-compact particles composed of aggregated monomers, regarding the mean  
330 scattering function convergence and the dispersion of the individual scattering function, no direct  
331 dependency of the number of necessary measurements with the fractal dimension is detected. Also,  
332 the results for the compact Gravel and the GravelPlexi particles are similar, which indicates  
333 that for our cases the refractive index has no effect on the number of necessary  
334 measurements when the imaginary part of the index indicates significant absorbing  
335 properties. For compact particles, the departure from the sphericity reduces the amplitude of  
336 Mie oscillations but has little effect on the number of necessary measurements. It seems that  
337 the surface roughness, or the size of the irregularities with respect to the wavelength, is the  
338 main parameter that drives the necessary number of measurements to retrieve the mean  
339 scattering properties. When the surface irregularities or the size of the monomers is below a  
340 critical value, probably smaller than about  $\lambda/5$  of the wavelength, they have no effect on the  
341 number of necessary measurements that have already reached a constant upper limit. The  
342 number of measurements evolves also with the deviation from the sphericity ( $D_i/D_v$   
343 parameter). When considering particles with size parameter greater than 2.5, to be above the  
344 transition from the Rayleigh scattering regime, the number of measurements reaches its  
345 maximum value for  $D_i/D_v > 2$  for intensity (accuracy at 1.5%) and  $D_i/D_v > 1.5$  for polarization  
346 (accuracy at 0.5%), as shown in Figure 10.

347 For the intensity, the 1.5% accuracy seems a good compromise between the number  
348 of necessary measurements and a desired accuracy in this size parameter range. The number  
349 of necessary measurements seems to reach an upper limit at about  $60 \pm 10$ . On the other hand,  
350 the fractal aggregates composed of small spherules exhibit small remaining Mie oscillations in  
351 the scattering curves even if the number of measurements is large. They produce the small  
352 undulations of about 1% shown in Figure 7 for more than 70 number of measurements, which  
353 are difficult to totally remove (more than a hundred of different orientations could then be  
354 necessary). For the polarization, an upper limit of  $70 \pm 10$  necessary measurements is enough  
355 to reach an accuracy of 0.5% in absolute value.

356  
357



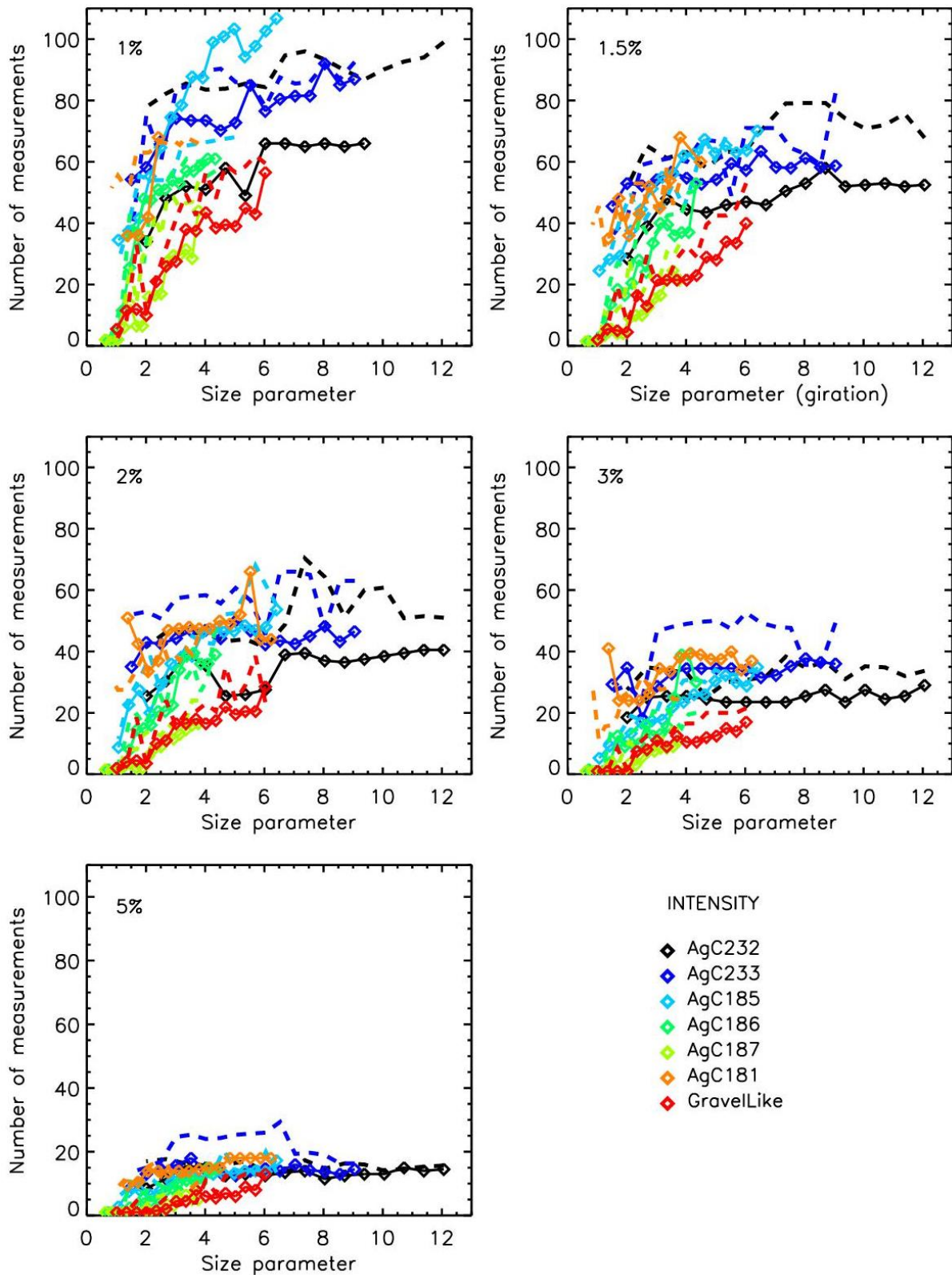
358  
 359 *Figure 10: Evolution of the number of measurements as a function of deviation from*  
 360 *sphericity ( $D_i/D_v$ ) for particles with size parameter greater than 2.5, for intensity (accuracy at*  
 361 *1.5%) and for polarization (accuracy at 0.5%)*

362  
 363  
 364 **4.2 Numerical calculations**

365  
 366 Numerical calculations of the scattering properties of the AgC181, AgC185, AgC186,  
 367 AgC187, AgC232, AgC233 and GravelLike have been conducted using the Finite Element  
 368 Method presented in [30] and using the same files to describe the geometry of the objects  
 369 than the one used to print them. The scattering properties are computed considering the  
 370 similar orientations and inclinations of the sample as during the measurements, by steps of  
 371  $10^\circ$ . The same method as the one used for measurements is conducted to determine the  
 372 number of necessary measurements to retrieve the mean scattering properties.

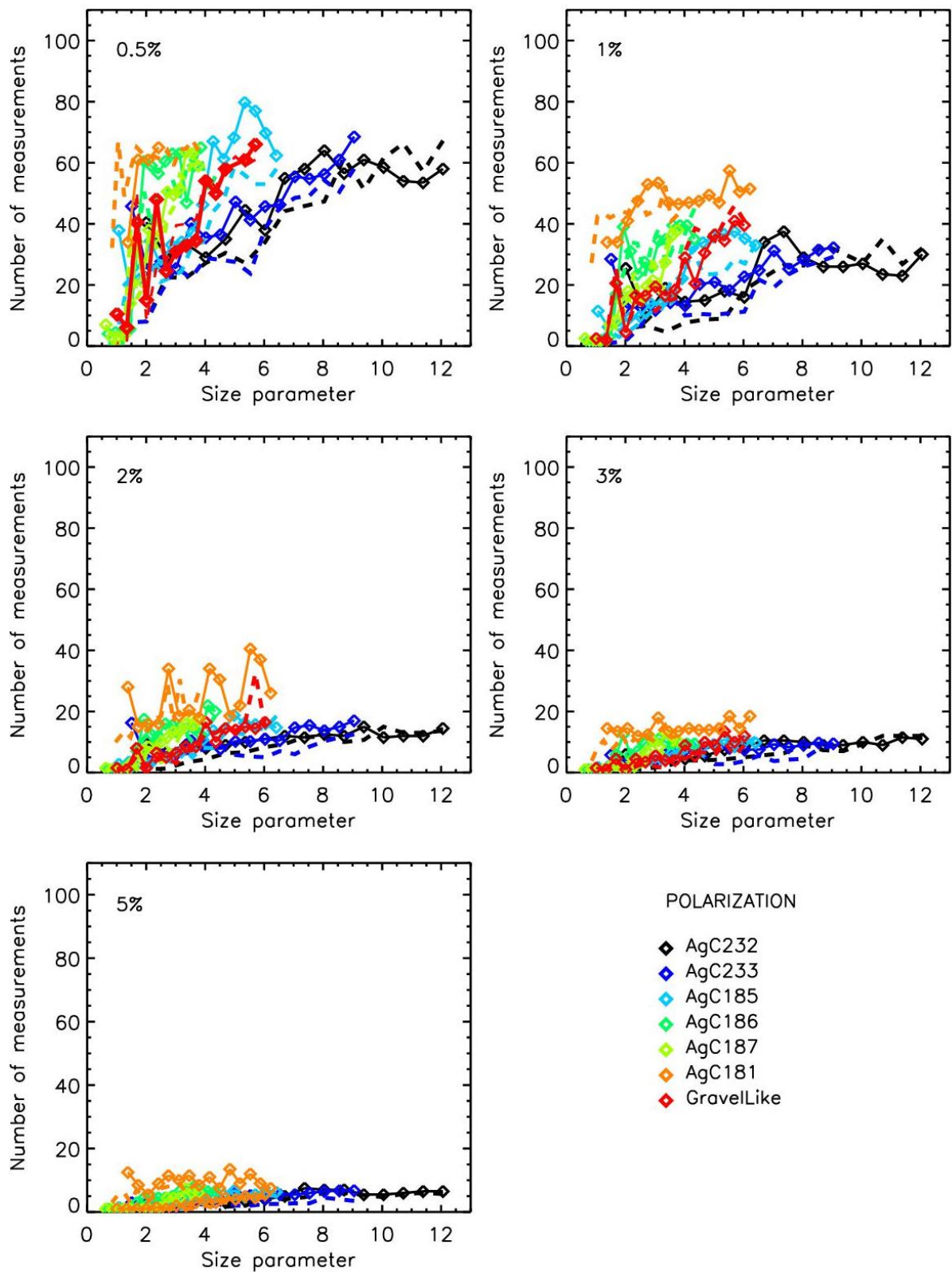
373 Figure 11 shows that theoretical calculations and microwave analogy measurements  
 374 have the same trends and are in correct agreement, considering the uncertainties.  
 375 Nevertheless, the model for the intensity often requires a larger number of orientations to  
 376 reach the same error as for the measurements. It seems that the model is more sensitive to  
 377 the remaining small Mie scattering oscillations than the measurements. The noise existing  
 378 naturally in the experiments can potentially help to reach more rapidly the random realization.  
 379 This effect seems less visible in polarization (Figure 12), confirming that intensity and  
 380 polarization are not sensitive to the same physical parameters of the particles. These results  
 381 confirm that such modelling calculations can be a good approach to retrieve the mean  
 382 scattering properties of fluffy and fractal particles when several tens of orientations are  
 383 considered.

384



385  
 386  
 387  
 388  
 389  
 390  
 391

Figure 11: Evolution of the number of necessary measurements with size parameter, to retrieve the intensity mean optical scattering properties, for different thresholds of uncertainties (the error bars of  $\pm 15\%$  for the number of necessary measurements are omitted for clarity). Full lines: measurements; dotted lines: modelling calculations.



392  
 393  
 394  
 395  
 396  
 397  
 398

Figure 12: Evolution of the number of necessary measurements with size parameter, to retrieve the polarization mean optical scattering properties, for different thresholds of uncertainties (the error bars of  $\pm 15\%$  for the number of necessary measurements are omitted for clarity). Full lines: measurements; dotted lines: modelling calculations.

399 The code uses a parallel direct sparse solver (Pardiso); the computation time and  
400 memory requirements are strongly related to the object studied and the size of its  
401 circumscribing box. Typically, for a run performed on a 28 cores SMP computer, the used  
402 memory varies between 7 GB (AgC187) to 80 GB (AgC232) while the run time varies between  
403 15 min (AgC187) to 11 hours (AgC232) for all frequencies. This calculation time for the  
404 particles studied here (fractals with less than 75 monomers) is much lower than the tens of  
405 hours necessary to retrieve experimentally the mean scattering properties from tens of  
406 different orientations. Thus, this numerical approach can be used in complement with real  
407 measurements to study the optical response of aggregates with various fractal dimension,  
408 number of monomers, shapes, and refractive indexes. On the other hand, experimental  
409 measurements could be the only solution to study particles having complex shapes (for  
410 examples with different size of monomers or highly variable surface heterogeneities) and to  
411 validate new numerical simulations methods or when the number of monomers or size of the  
412 objects is higher.

413

414

#### 415 4. Conclusions

416

417 The microwave analogy has allowed us to estimate how we can define the mean  
418 optical scattering properties of irregularly shaped particles observed with different  
419 orientations, and how they evolve with the size parameter. For all samples, the number of  
420 necessary measurements is between 10 and 20 to reach a mean scattering property with an  
421 uncertainty of 5% ( $1-\sigma$ ). Then, to reach a 1.5% error in intensity and 0.5% in polarisation, the  
422 number of necessary measurements strongly depends on the shape, the fluffiness, the  
423 deviation from a sphere, and the surface irregularities of the sample with respect to the  
424 wavelength (but not directly on their fractal dimension). For a slight rough sphere to a string-  
425 like aggregate of small monomers with a fractal dimension of 1.5, the number of necessary  
426 measurements increases from about  $20\pm 3$  to about  $70\pm 10$ . The higher value seems to be an  
427 upper limit.

428 Such results corroborate all the previous laboratory measurements of light scattered  
429 by clouds of levitating irregular randomly oriented particles where several tens of particles of  
430 the same size and having a size parameter below  $\sim 10$  are involved. They also show that  
431 considering several tens of orientations of the same particle might be sufficient for considering  
432 random orientation when performing modelling calculation for an aggregate composed of  
433 monomers, thus reducing the calculation time. Finally, new microwave analogy  
434 measurements could be conducted to better evaluate the effect of the surface roughness on  
435 the mean scattering properties of compact and fluffy particles, in particular for the small size  
436 parameters close to the transition to the Rayleigh scattering regime.

437

438 **Acknowledgments.** This work was partly funded by the French PRDA (“Plan Recherche et  
439 Développement Amiante”) supported by the French Ministry for the Ecological and Inclusive  
440 Transition and the Ministry for Regional Cohesion (SU 54-18-054), by the 2019 CNRS 80 Prime  
441 programme (project EXPERTS, EXploring Planet formation with lab ExpeRimentS), by the  
442 LOAC-Spatial project funded by the French Space Agency CNES, by the Centre Commun de  
443 Ressources en Microondes CCRM, and by the “Groupement de Recherche N°3622 SUIE”. The  
444 authors thanks F. Onifri for the DLA software dedicated to the generation of the aggregates.

445

446

## 447 **References**

448

449 1. Hadamcik E, Lasue, J, Levasseur-Regourd AC, Renard, JB. Analogues of interplanetary dust  
450 particles to interpret the zodiacal light polarization. *Planet Space Sci* 2020;183:104527.

451

452 2. Levasseur-Regourd AC, Baruteau C, Lasue J, Milli J, Renard JB. Linking studies of tiny  
453 meteoroids, zodiacal dust, cometary dust and circumstellar disks. *Planet Space Sci*  
454 2020;186:104896.

455

456 3. Levasseur-Regourd AC, Renard JB, Hadamcik E, Lasue J, Bertini I, Fulle M. Interpretation  
457 through experimental simulations of phase functions revealed by Rosetta in 67P dust coma.  
458 *Astronomy Astrophys* 3019;630:A20. DOI:10.1051/0004-6361/201834894.

459

460 4. Frattin E, Muñoz O, Moreno F, Nava J, Escobar-Cerezo J, Gomez Martin JC, Guirado  
461 D, Cellino A, Coll P, Raulin F. Experimental phase function and degree of linear polarization of  
462 cometary dust analogues. *MNRAS* 2019 ; 84P :2198–2211. DOI :10.1093/mnras/stz129.

463

464 5. Muñoz O, Moreno F, JGómez-Martín JC, Vargas-Martin F, Guirado D, Ramos  
465 JL, Bustamante I, Bertini I, Frattin E, Markannen J, Tubiana C, Fulle M, Güttler C, Sierks H,  
466 Rotundi A, Della corte V, Ivanovski SL, Zakharov VV, Bockelée-Morvan D, Blum J, Merouane S,  
467 Levasseur-Regourd AC, Kolokolova L, Jardiel T, Caballero A. Experimental Phase Function and  
468 Degree of Linear Polarization Curves of Millimeter- sized Cosmic Dust Analogs. *Astrophysical J*  
469 *Suppl* 2020; 247:19. DOI: 10.3847/1538-4365/ab6851.

470

471 6. Milli J, Engler N, Schmid H, Olofsson J, Menard F, Kral Q, Boccaletti A, Thébault P, Choquet  
472 E, Mouillet D, Lagrange AM, Augereau JC, Pinte C, Chauvin G, Dominik C, Perrot C, Zurlo A,  
473 Henning T, Beuzit JL, Avenhaus H, Bazzon A, Moulin T, Llored M, Moeller-Nilsson O, Roelfsema  
474 R, Pragt J. Optical polarised phase function of the HR 4796A dust ring. *Astron. Astrophys.* 2019;  
475 626:A54, DOI: 10.1051/0004-6361/201935363.

476

477 7. Andersson BG, Lazarian A, Vaillancourt JE. Interstellar dust grain alignment. *Ann. Review*  
478 *Astron. Astrphys.* 2015; 53:1, 501-39.

479

480 8. Daugeron D, Renard JB, Gaubicher B, Couté B, Hadamcik E, Gensdarmes F, Basso G, Fournier  
481 C. Scattering properties of sands, 1. Comparison between different techniques of  
482 measurements/ *Applied Opt* 2006;45:8331-37.

483

484 9. Maconi G, Penttilä A, Kassamakov I, Gritsevich M, Helander P, Puranen T, Salmi A,  
485 Hæggström E, Muinonen K. Non-destructive controlled single-particle light scattering  
486 measurement. *J Quant Spectrosc Radiat Transf* 2018; 204:159-64.

487

488 10. Renard JB, Worms J-C, Lemaire T, Hadamcik E, Huret, N. Light scattering by dust particles  
489 in microgravity: polarization and brightness imaging with the new version of the PROGRA2  
490 instrument. *Appl Opt* 2002; 41(4):609-18.

491

- 492 11. Renard JB, Hadamcik E, Couté B, Jeannot M, Levasseur-Regourd AC. Wavelength  
493 dependence of linear polarization in the visible and near infrared domain for large levitating  
494 grains (PROGRA2 instruments). *J Quant Spectrosc Radiat Transf* 2014; 146:424-30.  
495
- 496 12. Hovenier JW, Volten H, Muñoz OK, Van der Zande W, Waters LB. Laboratory studies of  
497 scattering matrices for randomly oriented particles: potentials, problems, and perspectives. *J.*  
498 *Quant. Spectrosc. Radiat. Transf* 2003; 79-80:741-55.  
499
- 500 13. Volten H, Muñoz O, Rol E, de Haan JF, Vassen W, Hovenier JW. Scattering matrices of  
501 mineral aerosol particles at 441.6 and 632.8 nm. *J. Geophys Res* 2001; 106(D15):17375-01.  
502
- 503 14. Muñoz O, Moreno F, Guirado D, Dabrowska DD, Volten H, Hovenier JW. The Amsterdam-  
504 Granada Light Scattering Database. *J Quant Spectrosc Radiat Transf* 2012; 113(7):564-74.  
505
- 506 15. Mishchenko MI, Yurkin MA. On the concept of random orientation in far-field  
507 electromagnetic scattering by non-spherical particles. *Opt Lett* 2017; 42(3):404-97.  
508
- 509 16. Grimm H, Eatough DJ. Aerosol measurement: the use of optical light scattering for the  
510 determination of particulate size distribution, and particulate mass, including the semi-volatile  
511 fraction. *J Air Waste Manage Assoc* 2009; 59:101-07.  
512
- 513 17. Gao RS, Telg H, McLaughlin RJ, Ciciora SJ, Watts LA, Richardson MS, Schwarz JP, Perring  
514 AE, Thornberry TD, Rollins AW, et al. A light-weight, high-sensitivity particle spectrometer for  
515 PM2.5 aerosol measurements. *Aeros Sci Technol* 2016; 50:88–9.  
516
- 517 18. Renard J.B, Dulac F, Berthet G, Lurton T, Vignelles D, égou F, Tonnelier T, Jeannot M, Couté  
518 B, Akiki R. et al. LOAC, a light aerosols counter for ground-based and balloon measurements  
519 of the size distribution and of the main nature of atmospheric particles, Principle of  
520 measurements and instrument evaluation. *Atmos Meas Technol* 2016; 9:172142.  
521
- 522 19. Zerull RH, Gustafson BÅS, Schulz K, Thiele-Corbach E. Scattering by aggregates with and  
523 without an absorbing mantle: microwave analog experiments. *Appl Opt* 1993;32: 4088–100.  
524 <https://doi.org/10.1364/ao.32.004088>.  
525
- 526 20. Gustafson BÅS, Kolokolova L. A systematic study of light scattering by aggregate particles  
527 using the microwave analog technique: Angular and wavelength dependence of intensity and  
528 polarization. *J Geophys Res Atmos* 1999; 104:31711–20.  
529 <https://doi.org/10.1029/1999JD900327>.  
530
- 531 21. Sabouroux P, Stout B, Michel Geffrin J, Eyraud C, Ayranci I, Vaillon R, Selçuk N. Amplitude  
532 and phase of light scattered by micro-scale aggregates of dielectric spheres: Comparison  
533 between theory and microwave analogy experiments. *J Quant Spectrosc Radiat Transf* 2007;  
534 103:156–67. <https://doi.org/10.1016/j.jqsrt.2006.06.001>.  
535
- 536 22. Merchiers O, Geffrin JM, Vaillon R, Sabouroux P, Lacroix B. Microwave analog to light  
537 scattering measurements on a fully characterized complex aggregate. *Appl Phys Lett*  
538 2009;94:2–4. <https://doi.org/10.1063/1.3129196>.

539  
540  
541  
542  
543  
544  
545  
546  
547  
548  
549  
550  
551  
552  
553  
554  
555  
556  
557  
558  
559  
560  
561  
562  
563  
564  
565  
566  
567  
568  
569

23. Merchiers O, Eyraud C, Geffrin J-M, Vaillon R, Stout B, Sabouroux P, et al. Microwave measurements of the full amplitude scattering matrix of a complex aggregate: a database for the assessment of light scattering codes. *Opt Express* 2010;18:2056. <https://doi.org/10.1364/oe.18.002056>.
24. Vaillon R, Geffrin JM. Recent advances in microwave analog to light scattering experiments. *J Quant Spectrosc Radiat Transf* 2014;146:100–5. <https://doi.org/10.1016/j.jqsrt.2014.02.031>.
25. Vaillon R, Geffrin JM, Eyraud C, Merchiers O, Sabouroux P, Lacroix B. A new implementation of a microwave analog to light scattering measurement device. *J Quant Spectrosc Radiat Transf* 2011; 112:1753–60.
26. Yon J, Bescond A, Liu F. On the radiative properties of soot aggregates part 1: Necking and overlapping. *J Quant Spectrosc Radiat Transf* 2015; 162: 197-206.
27. Bond TC, Bergstrom RW. Light absorption by carbonaceous particles: and investigative review. *Aeros Sci Techn* 2006; 40: 27-67.
28. Draine BT, Lee HM. Optical properties of interstellar graphite and silicate grains. *Astrophys J* 1984; 285:89D.
29. van de Hulst H. Light scattering by small particles. John Wiley and Sons eds., New York (USA) 1957.
30. Saleh H, Charon J, Dauchet J, Tortel H, Geffrin JM. Microwave analog experiments on optically soft spheroidal scatterers with weak electromagnetic signature. *J Quant Spectrosc Radiat Transf* 2017; 196: 1-9.